# New Revealing of High-Impedance Fault Testing on Normally Loaded Distribution Feeders

Micah Fitzgerald, James Tuccillo, and Sukhdeep Singh
*Pacific Gas and Electric Company*

Gandhali Juvekar and Yanfeng Gong
*Schweitzer Engineering Laboratories, Inc.*

Presented at the
52nd Annual Western Protective Relay Conference
Spokane, Washington
October 28–30, 2025

# New Revealing of High-Impedance Fault Testing on Normally Loaded Distribution Feeders

Micah Fitzgerald, James Tuccillo, and Sukhdeep Singh, *Pacific Gas and Electric Company*
Gandhali Juvekar and Yanfeng Gong, *Schweitzer Engineering Laboratories, Inc.*

***Abstract*—High-impedance faults (HIFs) do not generate sufficient fault current for detection by conventional overcurrent protection, but such faults can still ignite fires. Generally, these faults range from a few milliamperes to a few amperes. With the increasing focus on wildfire mitigation, reliable detection of HIFs to prevent wildfires is one of the electric power industry's top priorities. To gain more insights into HIFs, further support the research effort, and verify existing HIF detection algorithms, Pacific Gas and Electric Company (PG&E) conducted staged HIF tests on distribution feeders with live load at various locations. The testing revealed some unique aspects of HIFs including the following:**

- **Involving the actual ground fault current return path from the fault location to the substation ground during staged testing is the most holistic way to study HIFs.**
- **Downed conductors do not necessarily generate drastic bouncing (sometimes none) to create varying arcing signatures. Some existing algorithms are based on this assumption.**
- **The faults were staged on two operational feeders with normal load. Such testing results in a realistic, more accurate fault current signature for testing protection algorithms without overfitting.**
- **The initial stage of vegetation contact is often purely a high resistance fault with varying resistance and no visible arcing. Subampere fault current flows over tens of minutes during this initial stage before the vegetation experiences arcing over its surface. The initial contact stage is critical to detect faults to prevent wildfires because once the carbonized vegetation starts arcing and burning, it becomes difficult to prevent fire ignition.**

**This paper presents the related test data to demonstrate and support the aforementioned phenomena. Using the information gained during the testing, we propose a new algorithm to detect the early stage of vegetation contact causing HIFs for a three-wire, unigrounded system.**

## I. Introduction

With the rising occurrence of wildfires in recent years due to power lines, the power industry has increasingly invested in wildfire mitigation solutions. These mitigation plans can include employing sensitive intelligent electronic device (IED) settings during fire season for fast detection and isolation [1], deploying electrical and mechanical sensors to detect hazardous conditions, enhancing vegetation management, and undergrounding of power lines, to list a few [2]. It has become obvious in recent years that there is no single, easy solution to wildfire mitigation; many layers are needed to adequately reduce risk on power systems. One area that has continued to challenge these efforts is that of high-impedance faults (HIFs).

HIFs are one of the most complicated and widely researched types of faults. They are very challenging to detect with traditional overcurrent protection and can go undetected for hours or days, which often allows them to ignite fires and endanger public safety. HIFs, as the name suggests, are faults with impedance in the range of hundreds to thousands of ohms, limiting the fault current magnitude. Common HIF causes include tree branches touching wires and broken conductors landing on vegetation or other high-impedance surfaces. These HIFs often do not draw sufficient current for traditional overcurrent elements to pick up. Setting overcurrent elements to be sensitive enough to detect these events is not always an option as it may cause misoperations during normal system conditions.

Additionally, different grounding configurations witness different HIF behaviors. Four-wire, multigrounded systems with large system unbalance reflecting in the ground current see very little change in ground current during HIFs. Sometimes their ground current even decreases in magnitude depending on the existing system unbalance characteristics, the phase involved in the fault, and the location of the fault. For such systems, ground overcurrent elements are rendered ineffective and more complex algorithms based on HIF characteristics are necessary for detection. For three-wire, unigrounded systems, the ground current is at low levels pre-fault but may not experience a significant increase during HIFs. Load-switching action may falsely get classified as a fault if sensitive ground current elements are used without being qualified by other HIF characteristics to detect the faults [3].

HIFs can be viewed as a complex dynamic process that can involve conductor movement, a change in the material characteristics during the fault, rapid arc formation and extinction, and arc movement with changing arc length. Even advanced digital simulation techniques have challenges in simulating these features of an HIF [4]. As previously mentioned, extensive research has been carried out on this topic. Some researchers have pointed toward using third and higher odd harmonics for detecting arcing signatures [5] [6] [7] [8] while others have indicated using interharmonics for detection [4]. Some research uses statistical methods to detect HIFs [9] [10]: one such method uses high-frequency current components [11] and another uses burst noise signals near 60 Hz [12]. There has also been some interest in wavelet-based detection methods [13] and, more recently, in machine learning-based algorithms [14]. There is no shortage of methods for HIF detection, but the actual application, accuracy,

dependability, and security of these methods need much more real-world testing.

What causes this disconnect between current HIF detection methods and the reality of the field? For one, many approaches have been developed using data from staged faults in a laboratory setting without load or a real-world ground fault return path. Additionally, methods are often proposed with little testing using in-service distribution feeders to avoid any disruptions to service during testing. These factors lead to algorithms being developed using clean, or ideal, data, which do not represent real-world HIF scenarios. Second, because HIFs do not generate significant fault current, measurements from protection current transformers (CTs) lack precision and are likely to output inaccurate crucial information (e.g., inaccurate harmonics) rather than the accurate information that is required by these algorithms for detection. Lastly, usage of various signal processing methods may warp the data by exaggerating certain fault features in the ideal fault data used to develop these methods. These features may not reflect real-world data.

This prompted the authors of this paper to take a closer look at the problems of data collection, algorithm development, and continuous improvement of developed algorithms through actual system validation. We developed an edge-computing and data collection system to gather real-world data by continuously recording current and voltage on distribution feeders. This system records data during both normal load conditions and HIF conditions, over an extended period, for study and analysis. The heart of the system is a computing platform that can not only record weeks' worth of high-frequency sampled data, but also runs protective algorithms. Algorithms can be developed, revised, and tested nimbly with an edge-computing device like this.

This system was deployed on two Pacific Gas and Electric Company (PG&E) feeders connected to a substation with a three-wire, unigrounded configuration. Data were collected, studied, and used to develop and improve algorithms, which were then deployed back on the system, further improving the detection system. Fig. 1 shows a block diagram of the setup for data collection, research, and software updates using the IED, computer, and cell radio.

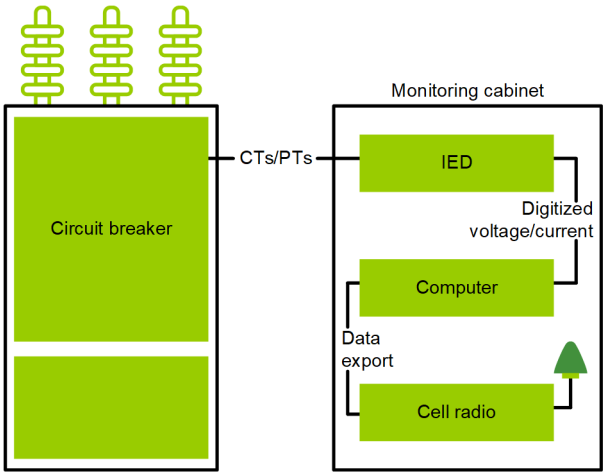


Fig. 1. An example of the edge-computing and data collection setup.

To further cement the effectiveness of developed algorithms and study various kinds of HIFs, we performed a variety of staged fault tests on the two live, in-service feeders. The goal was also to learn more about the early stages of faults, which often go undetected until the fault has progressed further. The capability to observe and study the initial state of the fault eventually led to the development of a new algorithm for detecting HIFs in the early stages to reduce wildfire risk.

The rest of the paper is structured as follows: Section II describes the setup used for testing faults on live feeders, and Section III details test results. Section IV describes early-stage, wire-in-branch fault characteristics, leading to the proposition of a new detection algorithm, and Section V details the results of the algorithm applied to two events.

## II. Staged Fault Test Setup

Our primary objective was to create and analyze HIFs under conditions that closely resemble real-world scenarios. While laboratory-based HIF testing has produced valuable insights over the years—thanks to the controlled environment and ideal monitoring conditions—it does not fully capture how HIFs interact with operational power systems under load. This study aimed to bridge that gap by examining fault behavior as observed by primary protection equipment in the field.

Field-based staged fault testing was conducted for two key reasons: 1) IED response analysis to observe how primary protective IEDs detect fault current at both the fault location and the substation source and 2) fault characterization to evaluate how fault current and characteristics vary based on factors such as distance from the source, terrain, fault surface, and ground conditions.

### *A. System Configuration*

This study focuses on three-wire, unigrounded distribution systems operating at 12.47 kV (line-to-line). These systems are grounded at a single point—typically at the substation transformer. In this study, the transformer was configured Y-Y grounded with a solidly grounded connection on the distribution side. Beyond the substation, only the phase conductors extend into the field, with no neutral wire. All supplied loads are connected phase-to-phase.

Because there is no zero-sequence path for load current, this configuration results in minimal standing residual current. Any residual current present is primarily due to line-to-earth capacitance imbalance, due to single-phase lines, or a CT mismatch, which can produce artificial residual current as measured by system IEDs. In such systems, line-to-ground faults rely on the earth as the return path for fault current.

### *B. Data Collection*

The data collection system as described in Section I and shown in Fig. 1 was installed at the distribution substation feeding both feeders involved in the staged faults. An IED was wired into the CT and potential transformer (PT) circuit of each feeder breaker to digitize the signals. Then, the IED streamed the current and voltage signals (sampled at 2 kHz) to a

computer to store the data. The data could be extracted from the computer locally or remotely via a cellular router.

### C. Fault Test Apparatus

The fault test apparatus consisted of multiple stages arranged in series.

#### 1) Primary Connection and Fuse Protection

One phase of the primary conductor was connected to a fuse cutout. The fuse was sized to coordinate with upstream system protection. This fuse served as a final safeguard to isolate staged faults and prevent customers from experiencing any outages from the testing. A cable connected the load side of the fuse to the next stage.

#### 2) Resistor Bank and Recloser

The next stage included a variable resistor bank to limit fault current. Integrated into the bank was a single-phase recloser, metering with a 50:5 CT into its 10 mA ground current input. The recloser provided manual control for the fault circuit. Protection on the recloser allowed low-current HIFs to remain energized for extended periods, while higher-magnitude faults were cleared quickly. This enabled prolonged fault observation under controlled conditions. Protection was set in three definite-time ground elements: 50 A for 0.05 seconds, 10 A for 3 seconds, and 4 A for 60 seconds. Protection was chosen to coordinate with the source-side fuse and to protect the resistor bank according to its rated power dissipation.

#### 3) Deionized Water Switch

An additional manual isolation method using a custom switch submerged in a tank of deionized water was included for enhanced safety and an additional open point.

### D. Fault Simulation

Two fault scenarios were tested as outlined.

#### 1) Wire on Ground

Wire-on-the-ground faults were simulated using a length of conductor suspended between two stands above the fault surface, as seen in Fig. 2. The fault area was enclosed in an aluminum arc box (8-inch tall plates) to contain step potential for personnel safety. The box was grounded via a single 1 ft long metallic construction stake. For the first scenario, aluminum stands were constructed at each end of the box and used to suspend a length of 1/0 aluminum conductor steel reinforced (ACSR) over the box and the soil below it. The conductor was insulated from the stands and arc box. A pneumatically actuated lever was used to lower the conductor to the ground or to simulate movement once the conductor was on the ground.

Fig. 2. Wire-on-ground apparatus at Location 2.

#### 2) Wire on Tree Branch

The second type of fault scenario simulated contact between an energized conductor and vegetation. For this setup, an additional aluminum stand was constructed as a table to hold a tree branch laying across it, as seen in Fig. 3. The tree branch rested on insulators and was isolated from the table. One end of the branch was connected to the source by wrapping a copper jumper wire around the branch. The other side of the branch was grounded to the arc box with another copper jumper wire.

Fig. 3. Wire-on-tree-branch apparatus at Location 2.

## III. Staged Fault Test Results

In total, 22 tests were performed across 3 days in differing weather conditions, at separate locations, on 2 distribution circuits, and using a variety of diverse fault media. The first day took place 50 ft outside the substation fence on Feeder 1, as seen in Fig. 4. The conditions were cloudy and cold with intermittent rain and hail. The soil was wet and rocky with sparse grasses and short weeds.

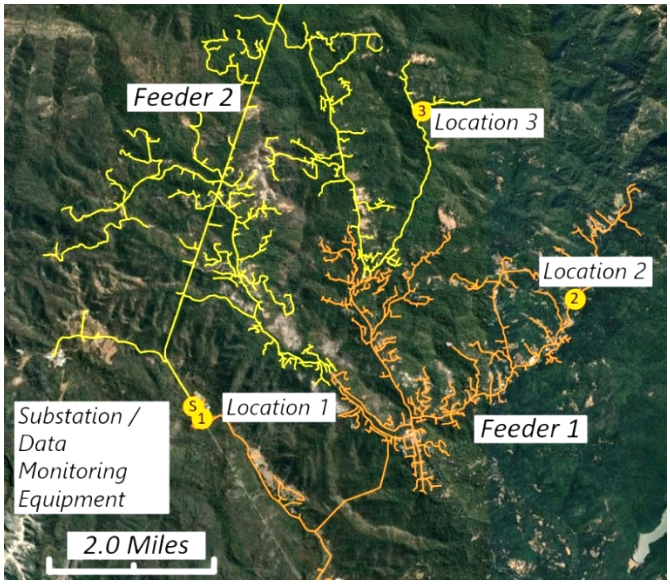


Fig. 4. Test locations on two distribution feeders showing the substation (also Location 1) and the two other test locations.

Table I contains the details of each test on the first day. During the wire-on-dirt testing, the fault amperes were limited by the resistor trailer. As seen in (1), the fault amperes were limited to 2 A, leaving the fault impedance at around 2 kΩ. Artificially adding to the fault impedance path is valuable in that it keeps the fault in the high-impedance range; however, it does not allow realistic fault progression because of how it limits fault current.

TABLE I
LOCATION 1 FAULT DETAILS

| Fault medium | Added resistance (Ω) | Fault duration (mm:ss) | Maximum rms current (A) |
|---|---|---|---|
| Wire on dirt | 1600 | 2:30 | 2 |
| Wire on dirt | 1600 | 2:18 | 2 |
| Wire on dirt | 800 | 3:00 | 3 |
| Manzanita branch | 800 | 6:00 | 0.01 |
| Redwood branch | 800 | 30:00 | 0.25 |
| Redwood branch with carbon dust | 800 | 30:00 | 2.5 |

$$Z_{fault} = \frac{V_{LN}}{I_{Fault}} - Z_{resistor\ bank} \quad (1)$$

$$Z_{fault} = \frac{7{,}200\ V}{2\ A} - 1{,}600\ \Omega = 2{,}000\ \Omega \quad (2)$$

Three branches were also tested during the first day. The manzanita branch had been collected several weeks prior to the testing and had dried out. It was soaked in water for 5 minutes prior to testing to simulate being in the wet conditions outside. After 6 minutes of applying voltage to the branch, there was no indication of any increase in current, and the test was ended. Our initial assumption was that the fault current would start to increase after a short amount of time; however, as would be seen later, each tree branch had a different fault profile, and many took a significantly longer time to conduct. Because of the dryness of the manzanita branch, we determined that it would remain insulative for longer than it was practical to test.

The next fault medium was a redwood branch collected on site several weeks prior and allowed to dry out. For 30 minutes, the branch was left faulted but the current never rose above 0.25 A and, eventually, it dropped to 0 A. The test was repeated with the same redwood branch but, this time, carbon dust from a burnt log was sprinkled on top. This dust was intended to provide a carbonized path for the fault current and to stimulate the fault development. This yielded good results as the fault current spiked up during the last 3 minutes of the fault (30 minutes total) at around 2.5 A. By the end, the branch was completely on fire and larger arcs were attempting to form but always died out. The arcs were pulsing in waves of intensity. It is postulated that the series resistor bank was limiting the fault current and not allowing the lower impedance fault to form. This test was manually ended.

The second day of testing was conducted on Feeder 1, 4.8 linear miles from the substation (Location 2). The weather was clear. The surface was gravel, still slightly damp from rain the day before. The first three tests involved the wire-down simulator. All three used 800 ohms of resistance. Immediately after the first test began, the fault current went to 7.5 A and stayed steady. The wire did not move but stayed on the ground steadily arcing until the recloser tripped after 22 seconds, as seen in Fig. 5. The second test was performed identically to the first with the wire in the same position and the fault current also spiked up immediately and the recloser tripped in 3 seconds.

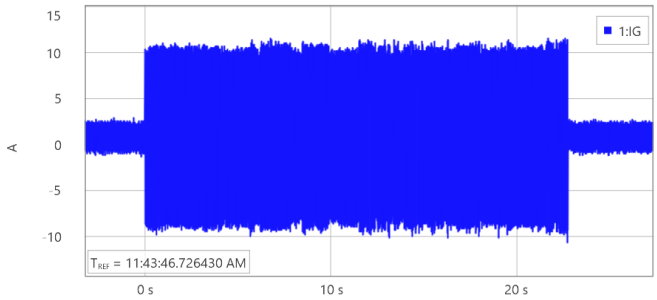


Fig. 5. Second day: first test with wire on dirt. The ground current rises to 7.5 $A_{RMS}$ immediately and stays there.

For the third test, a piece of dried sod was added underneath the conductor, simulating the wire falling on dry grass. The grass added extra impedance, but it quickly burnt and the sand in the sod melted. After 17 seconds, the fault returned to 7.5 A, and the recloser tripped after 1 minute, as seen in Fig. 6.

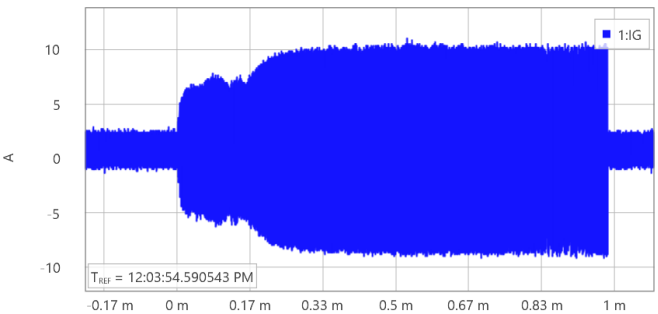


Fig. 6. Second day: third test with wire sod on dirt. The ground current rises to 7.5 $A_{RMS}$ after 17 seconds and stays there.

The next seven tests all utilized the tree branch fault simulator. Each one used a different variety of tree type. The first branch was collected off the ground already dead. It took significantly longer to catch on fire compared to the subsequent tests, likely because it was already dry. All the other branches were cut fresh, and they all took about 10 to 20 minutes to reach the recloser trip threshold of 4 A for 60 seconds. Each branch had a different fault profile, some starting to smoke sooner than others, some releasing more steam than others. During postanalysis, each branch type carried the fault differently as well, some in the bark, some in the outer wood, and some in the heart of the wood, as seen in Fig. 7. The smoke, burning, and arcing always began at the two ends of the branch, where it was grounded on one side and connected to the phase voltage at the other. Gradually, the burning and arcing traveled toward the middle of the branch and eventually met. When the carbon paths met, the fault impedance dropped dramatically. With the added 800 Ω of resistance, the fault current was limited, and the arcing continued at a lower level until it was interrupted by the slower protective element on the recloser.

(a)

(b)

(c)

(d)

Fig. 7. (a) Burnt fresh redwood with charring in the bark. (b) Burnt fresh madrone with burning and charring mostly under the bark in the inner wood. These holes were caused by high pressure steam escaping from inside the branch as it heated. (c) Madrone side view showing internal wood burnt. (d) Burnt fresh oak with both bark and inner wood burnt.

On the last test of the second day, the series fault resistance was removed entirely. This resulted in a dramatically different fault, as seen in Fig. 8. It only lasted three minutes and, during that time, the fault quickly ramped up. As the carbon path was completed, the fault hit 40 A and the recloser quickly tripped. Table II describes the fault details at Location 2.

Fig. 8. Last test at Location 2 with 0 ohms added series resistance. Final stages of the fault involved a violent explosion around the faulted branch.

TABLE II
LOCATION 2 FAULT DETAILS

| Fault medium | Added resistance (Ω) | Fault duration (mm:ss) | Maximum rms current (A) |
|---|---|---|---|
| Arc box with piston | 800 | 0:22 | 7.5 |
| Arc box with piston | 800 | 0:03 | 7.5 |
| Arc box with piston and dried sod | 800 | 1:00 | 7.5 |
| Moss- and lichen-covered oak branch | 800 | 23:45 | 0.01 |
| Freshly cut bay laurel branch | 800 | 10:00 | 5 |
| Freshly cut madrone | 800 | 10:00 | 5 |
| Freshly cut oak | 800 | 14:14 | 5 |
| Freshly cut redwood | 800 | 17:00 | 5 |
| Freshly cut eucalyptus | 800 | 12:00 | 5 |
| Freshly cut eucalyptus | 0 | 3:36 | 40 |

The last day of testing was performed on Feeder 2 at a location 4.5 linear miles from the substation. The weather was again clear. Location 3 was in a redwood forest, so the ground was moist and covered in a layer of redwood needles and some short grass. Six tests were performed at Location 3. The first three were with the wire-on-ground simulator, and the last three were with tree branches. For the wire-on-ground simulator, the series fault resistance was adjusted to 100 Ω to allow for a more true-to-life fault while still limiting the maximum fault amperes. All three tests were relatively short before being cleared by the recloser. After the first test, which only lasted 3 seconds, the conductor was raised higher above the ground and the actuator set up so that the conductor could be rapidly raised and lowered from the ground. This allowed the arc to form on the ground and then be drawn up into the air as the conductor was raised back up. This test provided data on highly active arcing faults. Dry sod was added under the conductor for the third test but, even then, the fault quickly progressed and the recloser cleared the fault after 33 seconds.

Next, three tests were performed with tree branches and the series fault impedance removed entirely. It was deemed acceptable to remove the fault impedance based on results from Location 2. The tree branch itself introduces enough impedance to limit the fault current until the branch has a complete carbonized path, then the fault becomes low impedance and the current quickly spikes up. The first branch test lasted for about 30 minutes before the branch burnt through and broke. After 12 minutes, and at only 0.25 A of fault current, the branch began to catch fire and by 0.5 A the branch was steadily burning from both ends. The current was only 1.3 A when the branch broke. The last test at Location 3 was different from all the other tests. This test is explained in detail in Section V. Table III describes the fault details at Location 3.

TABLE III
LOCATION 3 FAULT DETAILS

| Fault medium | Added resistance (Ω) | Fault duration (mm:ss) | Maximum rms current (A) |
|---|---|---|---|
| Arc box with piston | 100 | 0:03 | 20 |
| Arc box with piston, raised above ground | 100 | 0:10 | 20 |
| Arc box with piston, raised above ground over dried sod | 100 | 0:33 | 15 |
| Freshly cut bay laurel | 0 | 30:00 | 40 |
| Freshly cut bay laurel | 0 | 1:00 | 5 |
| Freshly cut redwood | 0 | 51:00 | 5 |

## IV. DETECTING AN EARLY-STAGE TREE-CONTACT HIF

As described in the previous section, various realistic high-impedance tests were performed on two feeders with a three-wire, unigrounded configuration. These tests yielded several observations:

- Different fault locations generated different fault current signatures, as expected, confirming the need to design tests at various feeder locations.
- Depending on the surface of contact, downed conductors may not experience drastic bouncing or movement due to low magnetic forces resulting from low currents. The fault may sometimes establish a steady arc and, hence, steady-looking current signature. Certain HIF algorithms are based on detecting varying arc signatures and fail to operate for such cases.
- With normal load still present on the system during testing, realistic fault signatures at the substation can be obtained. These fault signatures differ from the signatures obtained from ideal tests performed without system load considered, as waveforms only at the test location are obtained.
- Vegetation-related faults tend to be higher impedance than wire-down faults based on the testing performed.
- The main revelation of the tests was that when a wire touches a branch, the fault begins as purely resistive in nature. The faults on a three-wire, unigrounded system started off in the subampere range where the system unbalance existed and slowly increased in magnitude over tens of minutes, still maintaining the resistive nature. Initially, the heat generated by the fault expelled the water in the branch as steam for the first few minutes with an audible sound. Next, charring of the branch or bark began. The observation of the first two stages of steam expulsion and charring matches the findings in [15]. During these two stages of the fault, its resistive nature was observed. Once a carbonized path was fully established on the branch or bark, the nature of the fault became more erratic due to fluctuations in the arcing.

Fig. 9 highlights these observations, showing the gradual increase in ground current magnitude during the initial stages of the fault, slow decrease after the branch begins to dry, and finally the arcing stage where the current dramatically increases.

Based on our observations, we propose an algorithm to operate in the early resistive stage of the fault. The real power flow increasing trend between the faulted phase and ground that occurs due to the fault being resistive can be leveraged along with the real power flow decreasing trend between the nonfaulted phases and ground. Additionally, the logic can be secured by two more factors: limiting the operating range of the algorithm to be below a ground current threshold and checking that the change in power factor is close to 1 during the fault.

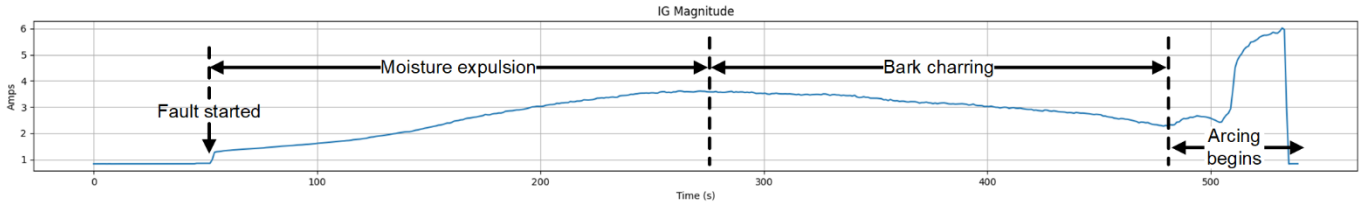


Fig. 9. Ground fault current signature for a madrone tree branch between a live phase and ground.

### A. Computing Real and Reactive Power

The following equations compute the effective real and reactive power flow between all phases and the ground.

$$P_{pG} = {\text{real}\left(V_{pPhasor} \bullet \overline{I_{GPhasor}}\right)}/{1{,}000}\,\text{kW} \quad (3)$$

$$Q_{pG} = {\text{imaginary}\left(V_{pPhasor} \bullet \overline{I_{GPhasor}}\right)}/{1{,}000}\,\text{kVAR} \quad (4)$$

where:

$\overline{I_{GPhasor}}$ is the complex conjugate of $I_{GPhasor}$
p = Phases A, B, and C

### B. Calculating Reference Values

The reference values used to compare the increase and decrease of quantities are moving average values. The reference values are computed for real and reactive power of each phase.

### C. Calculating the Power Factor Change

The power factor change quantity is computed for every phase and computes the increase in real power as compared to the increase in the apparent power. The goal of computing this quantity is to ensure that the power dissipated through the fault is mainly resistive.

### D. Detection Logic

A flowchart of the detection logic is shown in Fig. 10. The logic performs four checks, as shown in the figure, and starts incrementing a pickup counter when all four checks pass. When the pickup counter is greater than the counter threshold, a fault detection is declared for the phase the checks were run for. When any of the checks fail, the pickup counter is reset to zero. The checks performed are as follows:

1. The first check is to detect an increasing trend in the real power of Phase p, where p = A, B, or C, by comparing the real power against the sum of the moving average and a margin that can be decided using a setting generally set to detect an increase between 2 and 10 percent as compared to the reference or moving average value.
2. The second check is to detect a decreasing trend in the real power of the remaining two phases by comparing the real power against the moving average decreased by a margin that can be decided using a setting generally set to detect a decrease between 1 and 5 percent as compared to the reference or moving average value.
3. The third check is to detect that the power factor change is close to 1 by comparing it against a setting generally set between 0.85 and 0.99 to ensure that the power flow to ground is mainly real power.
4. The fourth check is to detect that the ground current is low and below a defined setting generally set between 1 and 5 A, so the logic only operates during the resistive stage of the fault.

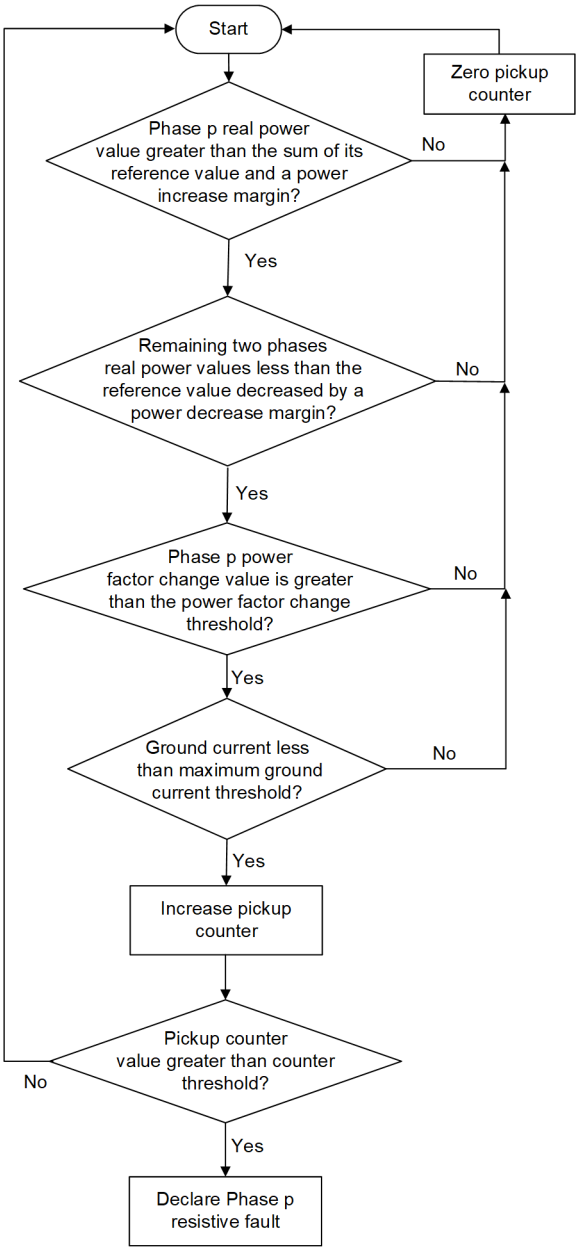


Fig. 10. Phase p resistive fault alarm logic, where p = A, B, or C.

## V. Early-Stage HIF Algorithm in Practice

As elaborated in Section II and Section III, various HIF tests were performed on two three-wire, unigrounded distribution feeders. Tests where the conductor was on ground surfaces like mud or grass showed more immediate changes in the ground current as compared to tests where the line was on a branch or a tree. The rise in ground current can take minutes, if not tens of minutes, and even then, the ground current is low for such vegetation contact scenarios. Algorithms using techniques like a change in harmonics or detection of variability in ground current fail to operate for these faults, but subampere current can still cause a fire, as demonstrated by the tests.

The logic in Fig. 10 is tested against these events where it is difficult to detect faults. Settings used were as follows: at least a 5 percent increase in real power of the faulted phase, at least a 2 percent decrease in the real power of the unfaulted phases,

a change in power factor greater than or equal to 0.95, and ground current below 2 A. If all the checks stay true for 10 seconds, which is the counter threshold, a fault is declared.

### *A. Event 1: Oak Branch Between Phase-C Wire and Ground*

The first event is on an oak branch between Phase C and ground on Feeder 1, which was the seventh event on Day 2, as seen in Table II. The event is 14 minutes long. The first 300 seconds see a slow and steady rise in ground current to around 1.95 A, as moisture in the bark is expelled, followed by a slow and steady drop in ground current for 100 seconds to around 1.8 A, as the branch starts charring. After this, the current rises more rapidly and variability in ground current can be seen as multiple arcs and flames form on the surface of the branch. At this point, the branch could easily have started a larger fire depending on the surrounding conditions. See Fig. 11a for the previously described ground fault current signature. See Fig. 7d for the branch after testing was finished. As the fault is Phase C, relevant plots with respect to Phase C are shown. Fig. 11b, Fig. 11c, and Fig. 11d show the real power flow between the phases and the ground for all three phases. For a Phase-C fault, an increase in the real power flow to the ground is seen when the fault starts at around the 1:20 minute mark, which satisfies the real power increase criteria in Fig. 10. The other two phases, A and B, see a decrease in real power flow at the same time and satisfy the real power decrease criteria for the unfaulted phases. Next, in Fig. 12, the power factor change in the faulted phase C goes close to one after the fault starts, while for the other two phases, it does not. Unfaulted Phases A and B do not pick up, as expected. Phase C picks up immediately after the fault starts when all required conditions are true and alarms once the pickup counter crosses the counter threshold of 10 seconds. The pickup drops when IG current magnitude crosses 2 A around the 500 seconds mark. The algorithm would have successfully avoided ignition of the branch had it been deployed on the system.

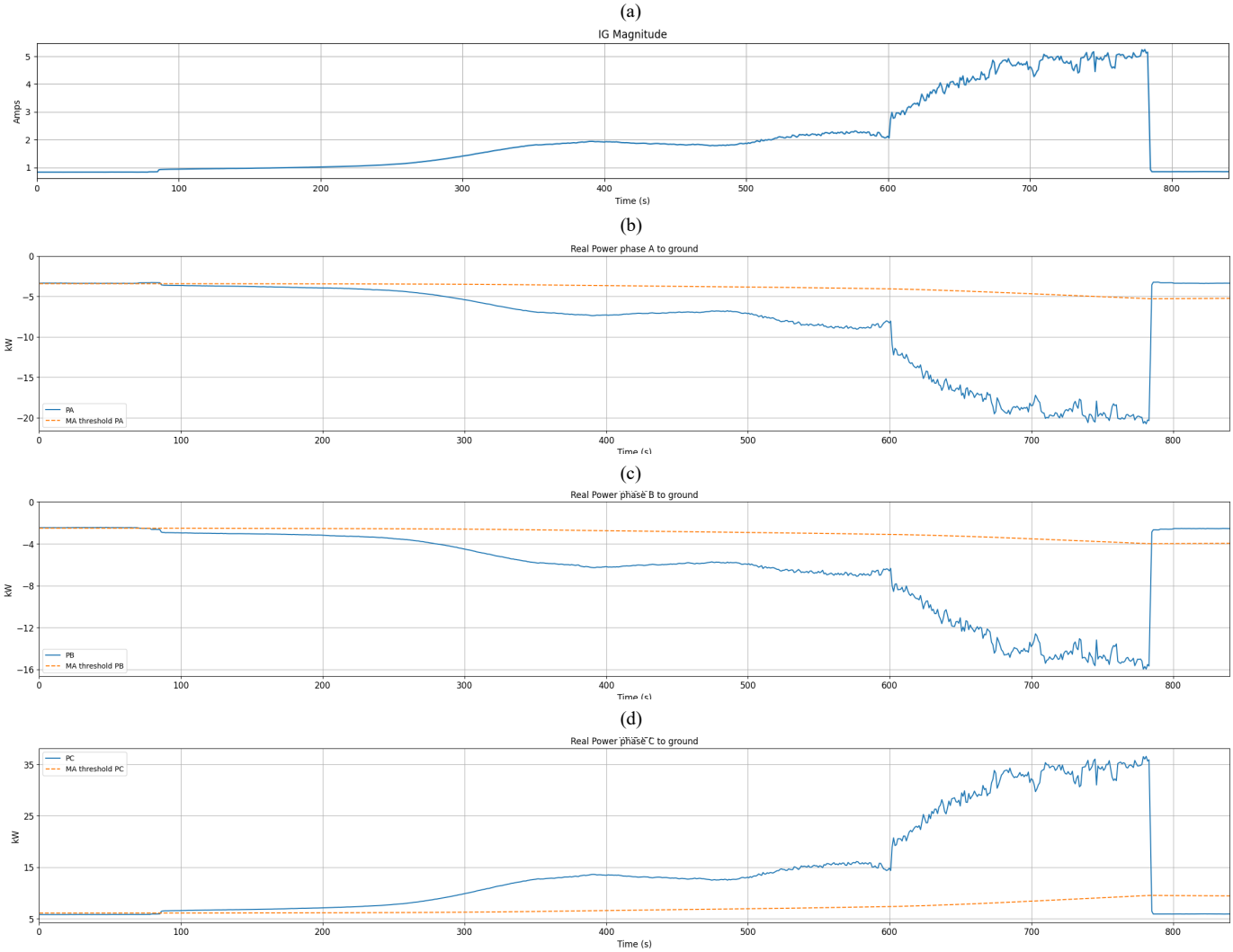


Fig. 11. (a) Ground fault current signature for an oak tree branch between Phase C and ground. (b) Real power flow between Phase A and ground with the real power decrease threshold. (c) Real power flow between Phase B and ground with the real power decrease threshold. (d) Real power flow between Phase C and ground with the real power increase threshold.

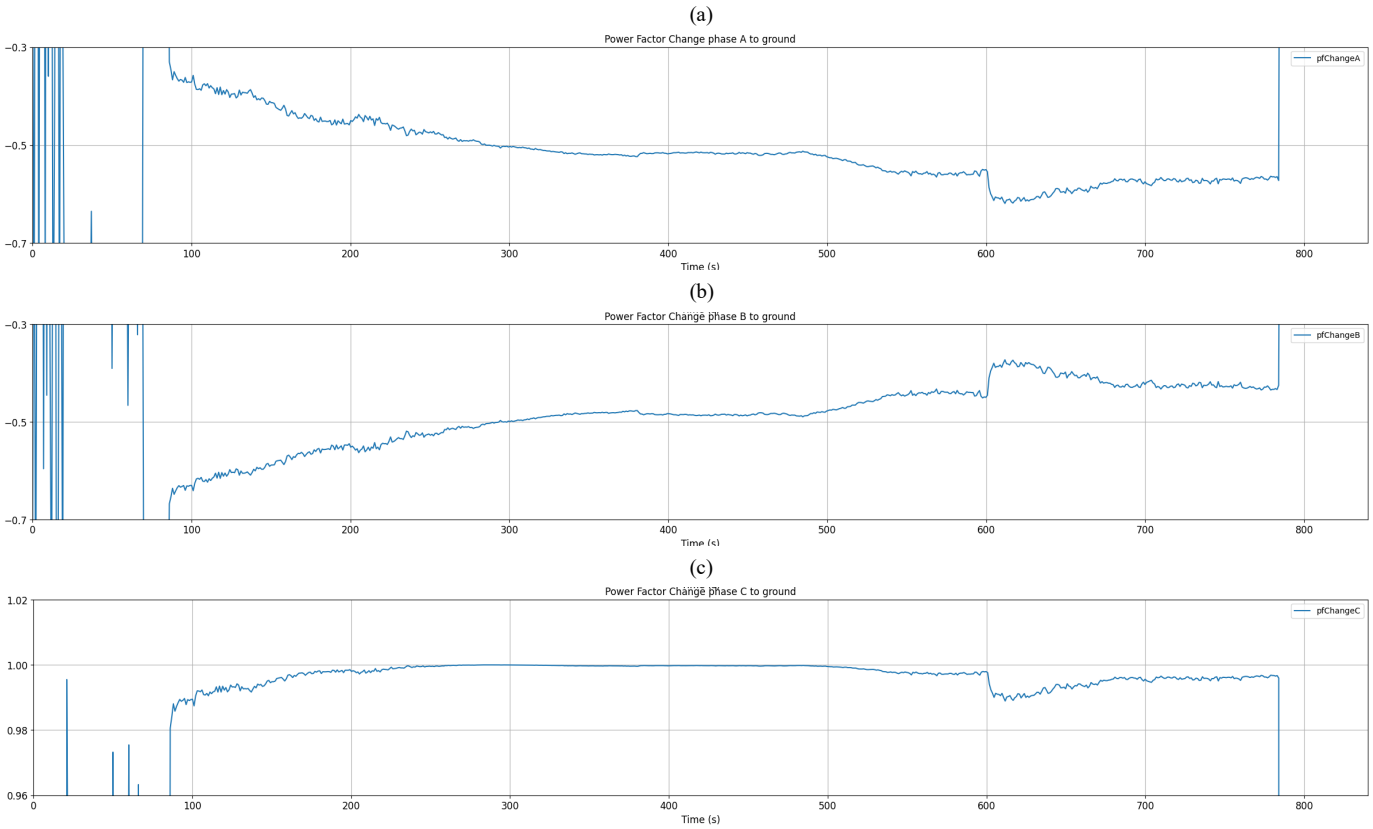


Fig. 12. (a) Power factor change for Phase A to ground. (b) Power factor change for Phase B to ground. (c) Power factor change for Phase C to ground. Zoomed in to show detailed changes.

### *B. Event 2: Long Redwood Branch That Mimics a Small Tree Between Phase-C Wire and Ground*

Following is the description of the test and results on a long redwood branch that mimics a small tree between Phase-C wire and ground. See Fig. 13. This was the last event on Day 3, as seen in Table III. The event is on Feeder 2 on a redwood branch between Phase C and ground. The event is 52 minutes long. For the first 20 minutes, a slight decreasing trend is observed in the actual ground current magnitude in Fig. 14a but the power flow from Phase C to ground actually sees a steady increase as seen in Fig. 14d, which then reflects in the real power flow from Phase C to ground. During this time, steam is expelled from the bark. After 20 minutes, the bark starts charring for a few minutes. At around the 25-minute mark, arcing starts, though the current is still low, indicating that as the branch or tree gets charred, arcs can start forming on the surface even at lower current. At around the 46-minute mark, it appeared as though the entire branch was on fire due to multiple arcs forming on the surface, as seen in Fig. 13, even though the current measured is still less than an ampere. After this, the current rises more rapidly and variability in ground current can be seen even though the measured current is still below 5 A. As the fault is Phase C, relevant plots with respect to Phase C are shown. The real power increase criteria for the faulted phase C and real power decrease criteria for the unfaulted phases A and B are met, as seen in Fig. 14b, Fig. 14c, and Fig. 14d, respectively. Next, the power factor change rises close to one after the fault starts for only Phase C, as seen in Fig. 15c, while it does not for the other two phases, as seen in Fig. 15a and Fig. 15b. As expected and desired, the logic alarms only on Phase C in 10 seconds, indicating an initial stage vegetation contact on Phase-C wire. The algorithm would have successfully avoided ignition of the branch, as seen in Fig. 13, had it been deployed on the system.

Fig. 13. Location 3: Image of the long redwood branch on fire due to multiple arcs forming on the surface.

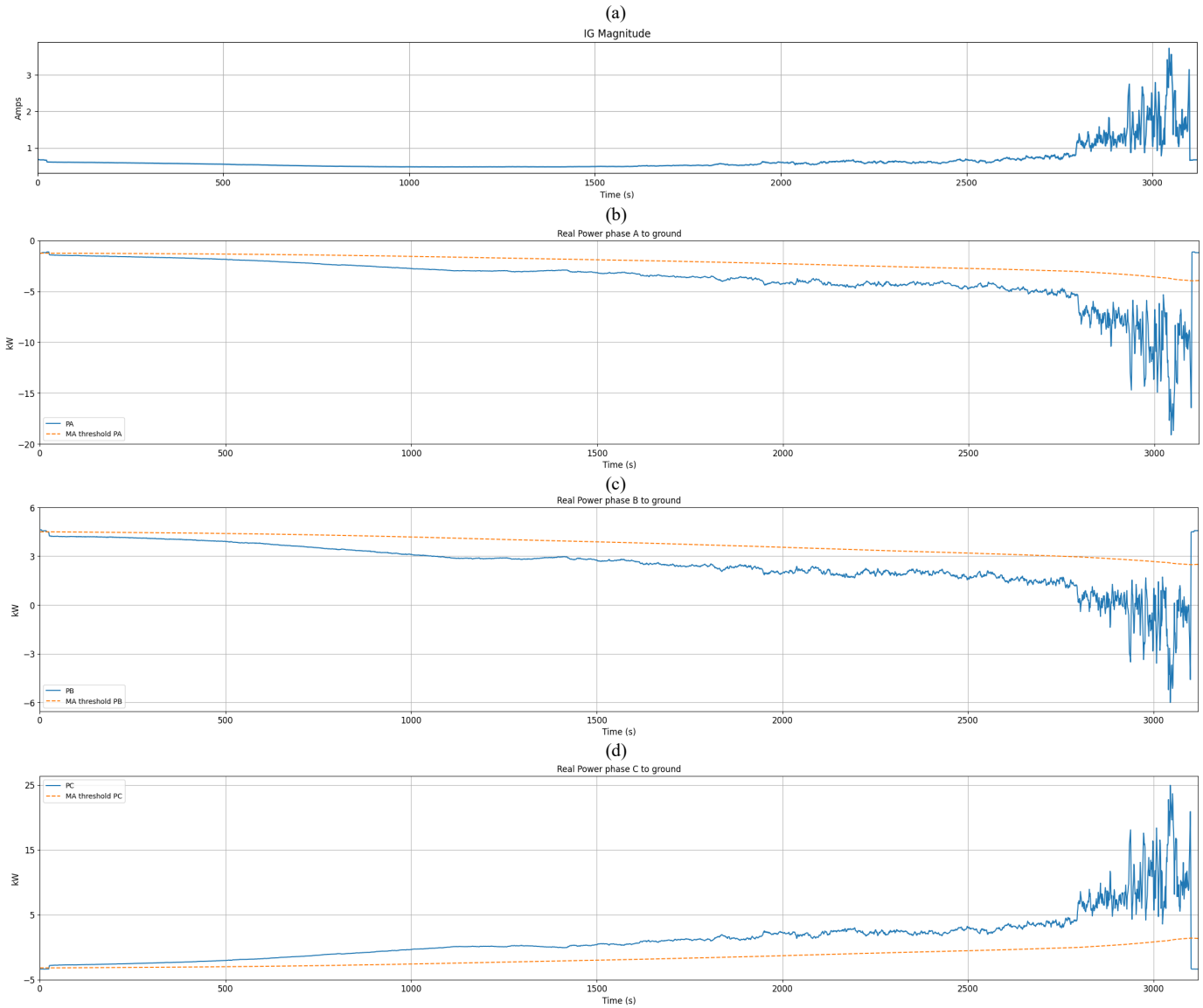


Fig. 14. (a) Ground fault current signature for a redwood tree branch between Phase C and ground. (b) Real power flow between Phase A and ground with the real power decrease threshold. (c) Real power flow between Phase B and ground with the real power decrease threshold. (d) Real power flow between Phase C and ground with the real power increase threshold.

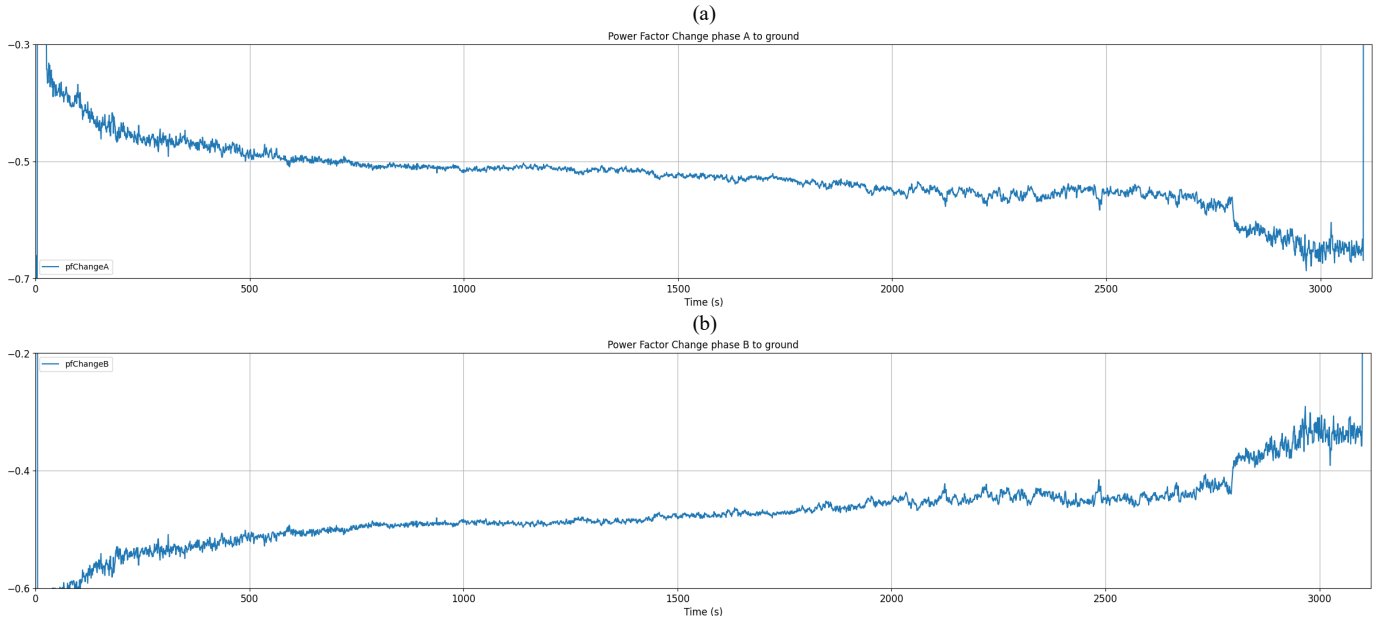

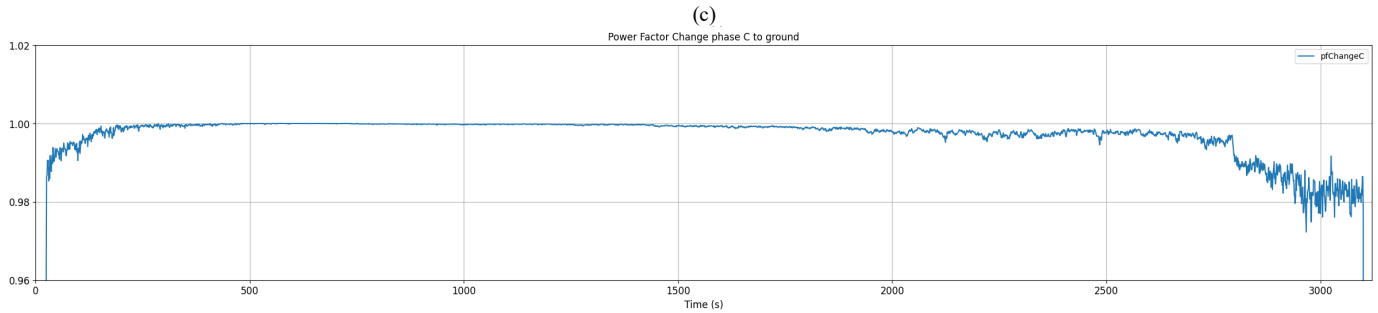


Fig. 15. (a) Power factor change for Phase A to ground. (b) Power factor change for Phase B to ground. (c) Power factor change for Phase C to ground.

This algorithm detected faults for all wires on branch- or tree-staged faults in Table II and Table III. As this section has demonstrated, a real power-based algorithm for detecting vegetation HIF faults in their early stages can be successfully deployed on an edge-computing device. This algorithm could be integrated into IED firmware, but firmware has a long development cycle and traditional microprocessor IEDs have many limitations including memory space for long event storage, inability to quickly patch firmware, and the need for a very rigid architecture so that core protective functions are always operational. The events studied in this paper lasted up to one hour, rendering traditional 1-second events at 16 samples per cycle useless. However, running this algorithm and others like it on an edge-computing device introduces enormous advantages like terabytes worth of event storage, allowing for minutes-long recordings at 2 kHz or higher sample rates, easy software patches to test and deploy new algorithms, and a separation of HIF detection from core protection functions (time overcurrent, reclosing, etc.). The main hurdle is communications between the IED and the edge-computing device, but with the advancement of digital substations, the hurdle is now only a small step to solve.

The research in this paper would have been impossible without an edge-computing system as described in Section I, and there is immense promise in using similar systems not just for research but for detection and system protection from HIFs.

## VI. Conclusion

This paper highlights the benefits of HIF field testing on operational distribution feeders using new edge-computing technologies with advanced data recording capability and advanced processing power for algorithm development and verification.

- A setup like this accomplishes various goals: extended data collection, which is reliable, real system events being captured for more than just a few seconds; the separation of HIF detection from core protection functions; and a nimble algorithm development process that allows for quick updates to algorithms, as the user is not locked to an IED's firmware.
- The HIF field testing helped obtain data at the substation through existing instrument transformers, thus capturing actual system load data and the ground return path. Various useful observations were obtained, like fault characteristics for ground contact and different branch contact, the maximum current, and the process of the fault progressing in a branch from moisture expulsion to complete burning.
- From the observations made during these staged tests that captured the slow-developing faults, the nature of the fault during the initial stage was characterized and an algorithm based on real power was proposed to detect it when the current is at subampere levels.
- Though the algorithm is for a three-wire, unigrounded system, the same burning characteristics of the vegetation occur on four-wire systems, and the algorithm proposed paves the way for the more complex, four-wire, multigrounded system HIF detection.
- The testing also validated the operation of various other later-stage algorithms that were developed using the data from the advanced recording setup.

## VII. References

[1] D. Taylor and K. Damron, "What's the Risk? One Utility's Approach to Strengthening Its Wildfire Resiliency," proceedings of the 48th Annual Western Protective Relay Conference, virtual format, October 2021.

[2] Pacific Gas & Electric Company, "Three-Year Wildfire Mitigation Plan Builds Upon Proven Layers of Protection, Includes Nearly 1,100 Miles of Undergrounding and Further Integration of New Technologies," April 2025. Available: investor.pgecorp.com/news-events/press-releases/press-release-details/2025/Three-Year-Wildfire-Mitigation-Plan-Builds-Upon-Proven-Layers-of-Protection-Includes-Nearly-1100-Miles-of-Undergrounding-and-Further-Integration-of-New-Technologies/default.aspx.

[3] J. Roberts, H. J. Altuve, and D. Hou, "Review of Ground Fault Protection Methods for Grounded, Ungrounded, and Compensated Distribution Systems," proceedings of the 28th Annual Western Protective Relay Conference, Spokane, WA, October 2001.

[4] D. Hou, "High-Impedance Fault Detection—Field Tests and Dependability Analysis," proceedings of the 36th Annual Western Protective Relay Conference, Spokane, WA, October 2009.

[5] D. I. Jeerings and J. R. Linders, "Unique Aspects Of Distribution System Harmonics Due to High Impedance Ground Faults," *IEEE Transactions on Power Delivery*, Vol. 5, Issue 2, April 1990, pp. 1,086–1,094.

[6] M. Farajollahi, A. Shahsavari, and H. Mohsenian-Rad, "Location Identification of High Impedance Faults Using Synchronized Harmonic Phasors," 2017 IEEE Power & Energy Society Innovative Smart Grid Technologies Conference (ISGT), Washington, DC, April 2017.

[7] E. A. Atwell, A. W. Shaffer, D. I. Jeerings and J. R. Linders, "Performance Testing of the Nordon High Impedance Ground Fault Detector On A Distribution Feeder," 34th Annual Conference on Rural Electric Power, Orlando, FL, 1990.

[8] A. Lazkano, J. Ruiz, E. Aramendi, L. A. Leturiondo, and J. A. González, "Study of High Impedance Fault Detection in Levante Area in Spain," *Ninth International Conference on Harmonics and Quality of Power Proceedings (Cat. No.00EX441)*, Vol. 3, October 2000, pp. 1,011–1,016.

[9] M. Ren and M. Baggu, "A New High-Impedance-Fault Detection Method to Prevent Power-Line-Induced Wildfires," 2024 IEEE Power and Energy Conference at Illinois (PECI), 2024.

[10] S. Gautam and S. M. Brahma, "Detection of High Impedance Fault in Power Distribution Systems Using Mathematical Morphology," *IEEE Transactions on Power Systems*, Vol. 28, Issue 2, May 2013, pp. 1,226–1,234.

[11] B. M. Aucoin and B. D. Russell, "Distribution High Impedance Fault Detection Utilizing High Frequency Current Components," *IEEE Power Engineering Review*, Vol. PER-2, Issue 6, June 1982, pp. 46–47.

[12] M. Aucoin and B. D. Russell, "Detection of Distribution High Impedance Faults Using Burst Noise Signals Near 60 HZ," in *IEEE Transactions on Power Delivery*, Vol. PWRD-2, Issue 2, April 1987, pp. 342–348.

[13] A.-R. Sedighi, M.-R. Haghifam, O. P. Malik, and M.-H. Ghassemian, "High Impedance Fault Detection Based on Wavelet Transform And Statistical Pattern Recognition," *IEEE Transactions on Power Delivery*, Vol. 20, Issue 4, October 2005, pp. 2,414–2,421.

[14] K. Rai, F. Hojatpanah, F. B. Ajaei, J. M. Guerrero, and K. Grolinger, "Deep Learning for High-Impedance Fault Detection and Classification: Transformer–CNN," *Neural Computing & Applications*, Vol. 34, April 2022, pp. 14,067–14,084.

[15] T. Marxsen, "Vegetation Conduction Ignition Test Report–Final," Powerline Bushfire Safety Program, Dept. Economic Development, Jobs, Transport and Resources, Technical Report, 2015.

## VIII. Biographies

**Micah Fitzgerald** works on the front lines of distribution protection strategy for wildfire mitigation at Pacific Gas and Electric Company (PG&E), especially related to high-impedance ground faults. He is responsible for developing and testing relay logic and settings for protective relays in the substation and on distribution lines. He works closely with multiple relay manufacturers to enhance and develop novel technologies for detecting high-impedance ground faults on distribution systems. He is also involved in designing and implementing automation and communications systems on the PG&E distribution system. Micah received his Bachelor of Science in Electrical Engineering from California Polytechnic State University, San Luis Obispo. He is an active member of IEEE Power & Energy Society (PES).

**James Tuccillo** is a leader within distribution operations and engineering with 15 years of utility power systems engineering experience in roles of increasing leadership. After spending the first half of his career in control center operations, James now manages the distribution engineering team at Pacific Gas and Electric Company (PG&E), which is responsible for capacity and reliability asset planning as well as distribution protection. He is currently the lead engineer on PG&E's Enhanced Powerline Safety Settings program, which has become a critical initiative to mitigate wildfire ignition risk on the distribution system. James is passionate about building teams and developing the next generation of engineers and leaders that will ensure that the future of the electric grid is able to safely deliver energy for customers and meet California's energy goals. James holds a bachelor's and master's degree in Electrical Engineering from California Polytechnic State University, San Luis Obispo, and is a registered professional engineer in California.

**Sukhdeep Singh** is an electrical engineering graduate from California Polytechnic State University, San Luis Obispo (class of 2020), with a Bachelor of Science degree and a focus in power systems. He is currently pursuing a California professional engineer (PE) license. Sukhdeep works at Pacific Gas and Electric Company (PG&E) as a distribution protection engineer, specializing in Research and Development projects related to protection systems and wildfire mitigation. He is experienced in developing standards for breaker control cabinets and line reclosers, supporting engineering teams in implementation, and assisting field crews with equipment installations.

**Gandhali Juvekar** received her Bachelor of Technology in Electrical and Electronics Engineering from the National Institute of Technology Karnataka (NITK), India, in 2017. She received her MS in Electrical Engineering from Texas A&M University, College Station, in 2019. She is currently a lead power engineer with Schweitzer Engineering Laboratories, Inc. (SEL). Her research interests include power system protection applications, time-domain quantities, geomagnetic disturbances, and distributed energy resources.

**Yanfeng Gong** earned his BS in Electrical Engineering with a specialization in power systems from Wuhan University, China, in 1998. He subsequently obtained an MS from Michigan Technological University in 2002 and a PhD from Mississippi State University in 2005. From 2005 to 2013, Yanfeng served as a research engineer at Schweitzer Engineering Laboratories, Inc. (SEL). He then transitioned to American Electric Power (AEP), where he was a principal engineer and supervisor in the Advanced Transmission Studies & Technologies (ATST) department from 2013 to 2019. In 2019, Yanfeng returned to SEL, currently assuming the role of fellow engineer in Research and Development. In addition to his professional endeavors, Yanfeng has been an active participant in industry committees. He served as the past chair of the IEEE Transient Analysis and Simulations Subcommittee (TASS) and is currently the chair of the IEEE Analytic Methods for Power Systems (AMPS) Technical Committee. Yanfeng is a Senior Member of the IEEE and a registered professional engineer (PE) in the state of Washington.